The effect of sulfidation on the Ni distribution in Ni/USY zeolites

ELSEVIER

The effect of sulfidation on the Ni distribution in Ni/USY zeolites

B. Pawelec and J.L.G. Fierro
Instituto de Catálisis y Petroleoquímica, CSIC, Campus UAM, Cantoblanco, Madrid, Spain

J.F. Cambra, P.L. Arias, and J.A. Legarreta
Escuela de Ingenieros Industriales, Bilbao, Spain

G. Vorbeck, J.W. de Haan, V.H.J. de Beer, and R.A. van Santen
Schuit Institute of Catalysis, Eindhoven University of Technology, Eindhoven, The Netherlands

Ni/USY zeolite catalysts have been prepared by either an ion-exchange or an impregnation procedure. The modification of support and the effect of sulfidation on the Ni distribution were examined by various techniques (water adsorption, *FT* i.r. spectroscopy of chemisorbed NO, XPS, ^{129}Xe n.m.r. and Xe adsorption). In all catalysts the sulfidation of Ni is incomplete and the method of Ni introduction influenced the Ni distribution in Ni/USY zeolites. In unsulfided samples ion-exchange technique led to Ni located essentially in hexagonal prisms, whereas in the other samples prepared by impregnation procedure the Ni concentrates were located at or near the outer zeolite surface. Some nickel redistribution has been observed during catalyst sulfidation.

Keywords: Ni/USY zeolite; *FT* i.r. of chemisorbed NO; XPS; ^{129}Xe n.m.r. spectroscopy; water and Xe adsorption

INTRODUCTION

Transition metal (TM)-loaded zeolites constitute one of the most interesting catalyst categories; they are useful for many hydrocarbon conversions, mainly because of the ability of the zeolite to function as a high surface area, acidic, and shape-selective catalyst support. In particular, industrial hydrocracking processes often combine zeolites and TM. This is due to the fact that the TM supported on zeolites yield lighter products and are more resistant to deactivation by N- and S-containing compounds than when supported on silica-aluminas.[1] The precise design of this type of catalyst is still difficult to discern because of the limited knowledge about the location, distribution, and interaction of the active ingredient with the zeolite surface as well as their implications on the catalytic performance.[2]

Several studies of zeolite Y-supported nickel sulfide have been reported in recent years.[3–14] Because USY has a lower ion-exchange capacity than NaY zeolite, a less uniform pore system, and contains extraframework alumina (EFAL), which might react with Ni to some extent, especially during calcination, Ni/USY systems are less well described than Ni/NaY catalysts. In general, the degree of nickel sulfidation or reduction was affected by the preparation procedure, by the extent of nickel exchange, and by the type of the nonexchanged cations. It has been found that Ni^{2+} ions located in hexagonal prisms (S_I sites) are less accessible to reducing or sulfiding agents than those in the supercages (S_{II}) and sodalite cages ($S_{I'}$, $S_{II'}$). The state of the sulfide ingredient was determined by using different chemical and physical probes by Cid et al.,[5] Kovacheva et al.,[6] Cornet et al.,[7] and Welters et al.,[8] who concluded that sulfidation was accompanied by an increase in Brönsted acidity. In the case of Ni/USY zeolite, Leglise et al.[9] and Ezzamarty et al.[10] found by photoelectron spectroscopy that Ni concentrates near the zeolite surface in calcined samples and that it became better dispersed upon sulfidation. Moreover, using *FT* i.r. of chemisorbed NO, Pawelec et al.[11] concluded that in sulfided Ni/USY zeolites a fraction of the nickel remains unsulfided.

In this paper we study the effect of the preparation method together with the effect of sulfidation on the Ni distribution in the USY zeolite. The difficulties of low ion-exchange capacity of the USY zeolite was overcome by increasing the Ni content using ion-exchange followed by impregnation techniques. As it seems to be of interest to identify the nature, location, and dispersion of sulfide phases brought about by sulfidation, as well as their interaction with the zeolite support, the present work is concerned with the physicochemical character-

Address reprint requests to Dr. Fierro at the Instituto de Catalisis y Petroleoquimica, CSIC, Campus UAm, Cantoblanco, 28049 Madrid, Spain.
Received 4 October 1996; accepted 27 November 1996

655 Avenue of the Americas, New York, NY 10010

0144-2449/97/$17.00
PII S0144-2449(97)00010-9

ization of sulfided Ni/USY catalysts. For this purpose, water adsorption, *FT* i.r. spectroscopy of chemisorbed NO, XPS, and ^{129}Xe n.m.r. spectroscopy in combination with xenon adsorption techniques are used to characterize both the precursor and sulfided nickel phases and their distribution throughout the zeolite particles.

EXPERIMENTAL

Catalyst preparation

All the nickel-containing zeolites were prepared from the original ultrastable Y zeolite. The characteristics of this USY zeolite are as follows: SiO_2/Al_2O_3 mole ratio 5.6, Na_2O content 0.14 wt%, and unit cell 2.454 nm. As the USY zeolite has low exchange capacity, only small amounts of Ni can be incorporated by the ion-exchange procedure. However, the Ni content incorporation can be increased by combining ion-exchange and impregnation procedures. Accordingly, one catalyst containing 1.4 wt% of Ni was prepared by ion-exchange from a 0.17 M aqueous solution of $Ni(NO_3)_2 \cdot 6H_2O$ (Merck, reagent grade), using a volume ratio of solution to zeolite of 20:1, at a constant temperature (333 K), and maintained with constant stirring for 24 h. The zeolite was separated by decantation, repeatedly washed with 50 cm^3 of distilled water, dried in air at 383 K for 4 h, and calcined at 723 K for 2 h. The other two catalysts containing 5.0 and 9.0 wt% of Ni were prepared by combining both ion exchange (in a similar manner as for the 1.4 Ni sample, except for the different nickel nitrate concentration) and impregnation (instead of decantation, a rotary evaporator was used for water removal). The subsequent drying and calcination steps were identical to those noted above. The catalysts will be referred to as *x*Ni, where $x = 1.4$, 5.0, and 9.0 denotes the wt% of Ni on a water-free zeolite basis.

Characterization techniques

The nickel content was determined by atomic absorption spectrometry using a Perkin-Elmer 3030 absorption instrument. The samples were solubilized in a mixture of HF, HCl, and HNO_3 and were homogenized in a microwave oven at a maximum power of 650 watts.

Pore volumes were calculated from the nitrogen adsorption isotherms, measured at 77 K using a Micromeritics Digisorb 2600 on samples that were previously outgassed at 623 K. Adsorption capacities of water were measured gravimetrically using a Cahn-2000 microbalance connected to a vacuum line and gas-handling system. A 70-mg unsulfided sample was used in each experiment, and the sensitivity was adjusted to 1 μg. Before water adsorption the samples were thoroughly outgassed under dynamic vacuum (ca. 1.2×10^{-5} torr, 1 torr = 133.3 Nm^{-2}) at 623 K for 14 h. Then they were cooled to ambient temperature (298 K) and were contacted with the adsorbate at relative pressures (P/P_o) between 0 and 1. The isotherms were constructed in gradual steps by increasing the pressure in small successive increments by evaporating distilled water from an ampoule sealed to the microbalance bottle. The equilibrium pressure was measured with a baratron MKS capacitance pressure transducer connected to the same vacuum line. The equilibrium was considered when the overall weight did not change more than 0.15% of the total amount of water already adsorbed.

Infrared spectra of adsorbed NO were taken with a Nicolet 5ZDX Fourier Transform Infrared spectrometer working with a resolution of 4 cm^{-1} in the whole spectral range. Infrared experiments were carried out in a cell provided with greaseless stopcocks and KBr windows, which allowed thermal treatments under vacuum. The zeolites (thickness 13.6–15.0 mg/cm^2) were first outgassed at 723 K under vacuum for 3 h. After cooling to room temperature, they were contacted with ca. 30 torr of NO, and the i.r. spectrum was recorded. Sulfided zeolites were also studied using NO as probe molecule. In all cases, the spectra were recorded after a 15-min exposure to NO at room temperature. The *in situ* sulfiding procedure was as follows: The samples were heated in a helium flow at 673 K for 0.5 h, then were exposed to a mixture of $H_2S:H_2 = 1:9$ for 3 h at the same temperature, followed by purging in a helium flow at 673 K for 0.5 h. Outgassing and chemisorption conditions were the same as above.

Photoelectron spectra were recorded with a Fisons ESCALAB 200R electron spectrometer equipped with a MgK_α X-ray source (hv = 1253.6 eV) and a hemispherical electron analyzer. The X-ray source was operated at 12 kV and 10 mA. The precursor and sulfided samples (sulfided *ex situ* in a $H_2S:H_2 = 1:9$ mixture at 673 K for 3 h) were pressed into small stainless steel cylinders (under isooctane in the case of sulfided samples to avoid contact with the air) and were mounted onto a manipulator, which allowed transfer from the preparation chamber into the analysis chamber of the spectrometer. The samples were pumped out to 10^{-5} torr before they were moved into the analysis chamber. The residual pressure in this ion-pumped chamber was maintained below 7×10^{-9} torr during data acquisition. Each spectral region of the photoelectrons of interest were scanned a number of times to obtain good signal-to-noise ratios. Although surface charging was observed on all the samples, accurate binding energies (±0.2 eV) could be determined by charge referencing with the adventitious C1s peak at 284.9 eV.

A Bruker MSL 400 spectrometer has been used for the ^{129}Xe n.m.r. measurements. The spectra were taken at 303 K at 110.7 MHz with pulse excitation (0.5-s pulse delay) on stationary samples. The number of scans was between 2×10^2 and 7×10^4. The chemical shift δ depending on the amount of xenon adsorbed per gram of dried and unloaded zeolite (xenon density), is given with respect to the value for gaseous ^{129}Xe, which is used as a reference. After pretreatment procedures (drying in helium for 2 h at 673 K; sulfidation in a mixture of $H_2S/H_2 = 1:9$ for 2 h at 673 K; heating rate = 6 K/min), the samples have been transferred via a recirculation-type glove box (O_2 and $H_2O < 2$ ppm) into the tubes used for xenon adsorption and n.m.r. spectroscopic measurements. The samples have been evacuated at 303 K ($p < 10^{-2}$ Pa) followed by a successive

adsorption of xenon at the same temperature (time of adsorption at each xenon pressure: 10 min).

RESULTS

Water sorption capacities

The shape of the adsorption isotherms for zeolites is not very informative and classical methods used to calculate the monolayer capacity do not work.[15] Thus, the obtained results of "BET" analogous surface area measurements on zeolites using nitrogen as an adsorbate cannot be considered as absolute and correct values, even though they may approach the real ones. As nitrogen adsorption does not involve specific interactions, the micropore volume can be calculated by applying the Polanyi-Dubinin theory. The water adsorption method seems, however, more attractive.[16] The polar character of water involves specific interactions between water molecules and hydrophilic centers, which are silanol groups or compensating cations.

The water sorption isotherms determined for various calcined (unsulfided) xNi samples at 298 K at relative pressures P/P_0 between 0 and 1 are displayed in *Figure 1*. For all catalysts the water isotherms exhibit a rapid increase in water adsorption at P/P_0 below 0.2, then increase slowly up to P/P_0 close to 0.8. By comparing the amounts of water condensed at $P/P_0 = 0.4$ (*Table 1*), it is apparent that the Ni-free zeolite shows the maximum sorption capacity. A very small decrease in sorption capacity is observed for the 1.4 Ni and 5.0 Ni zeolites and slightly larger for the 9.0 Ni homologue. This is expected because the micropore volume of the zeolite decreases with an increasing Ni percentage. The maximum volume (W_0) accessible to water was calculated from the Dubinin-Raduschkevitch (DR) equation.[16–18] In the linear form the DR isotherm is: $\log W = f[T.\log(P_0/P)]$. The ordinate at the origin of the line defines W_0. The linear transforms of the DR equation for the isotherms displayed in *Figure 1* are shown in *Figure 2*, and the W_0 values are compared in *Table 1* with the results of N_2 isotherms at $P/P_0 = 0.2$. The maximum W_0 and N_2 adsorption capacities are observed for the USY zeolite, but they decrease for *x*Ni samples. The strongest decrease is observed at the highest Ni content. Accordingly, both the N_2 sorption capacity and the maximum micropore volume of the zeolite accessible to water provide information about the presence of Ni within the zeolite pores.

Table 1 Water adsorption at 295 K ($P/P_0 = 0.4$) and N_2 adsorption at 78 K ($P/P_0 = 0.2$) for unsulfided *x*Ni USY zeolites

Zeolite	Ni (wt%)	W_0 (cm^3/g_{zeol})[a]	$V_{Nitrogen}$ (cm^3/g_{zeol})
1.4 Ni[b]	1.4	0.35	176
5.0 Ni[c]	5.0	0.34	165
9.0 Ni[c]	9.0	0.28	164
USY		0.37	185

[a] W_0 is the maximum volume of the zeolite accessible to water.
[b] The catalyst was prepared by ion exchange.
[c] The catalyst was prepared by ion exchange followed by impregnation.

Fourier transform infrared spectroscopy (*FT* i.r.)

Infrared spectroscopy of the NO molecule has been used to titrate the chemical environment of Ni^{2+} ions in both precursor and sulfided Ni-loaded zeolite catalysts.[11] The *FT* i.r. spectra of the NO chemisorbed on the precursor *x*Ni samples (*Figure 3A*) are compared with those of the sulfided counterparts (*Figure 3B*). Adsorption of NO on the precursor *x*Ni samples gave rise to a single band at ca. 1,900 cm^{-1}. In agreement with literature findings[19,20] this band is associated with the stretching vibration mode of the N-O bond in NO monomers chemisorbed on Ni^{2+} ions. The i.r. spectra of NO chemisorbed on sulfided catalysts are, however, more complex. They show two bands, one at ca. 1,900 cm^{-1} and an other at ca. 1,850 cm^{-1}; the latter is due to

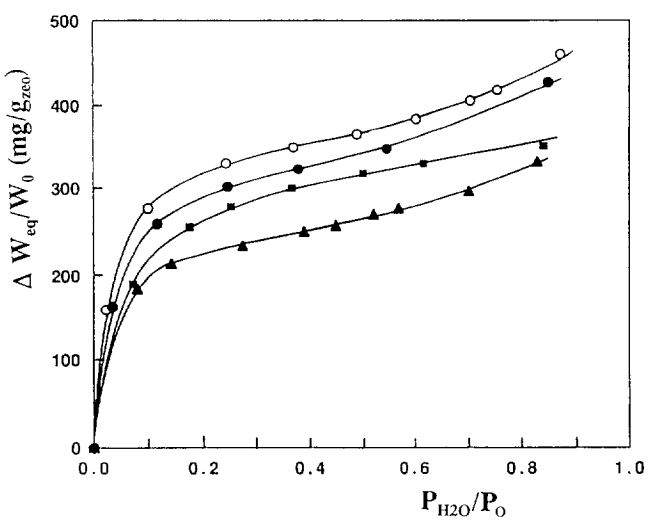

Figure 1 Adsorption isotherms of water at 295 K on different unsulfided *x*Ni USY zeolites: (○), USY; (●), 1.4 Ni; (■), 5.0 Ni; (▲), 9.0 Ni.

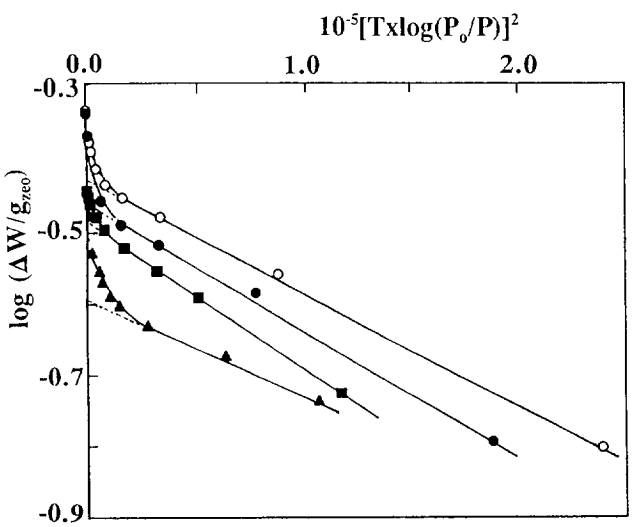

Figure 2 Dubinin-Raduschkevitch transforms for the adsorption isotherms of water at 295 K on unsulfided *x*Ni USY zeolites. The symbols are the same as in *Figure 1*.

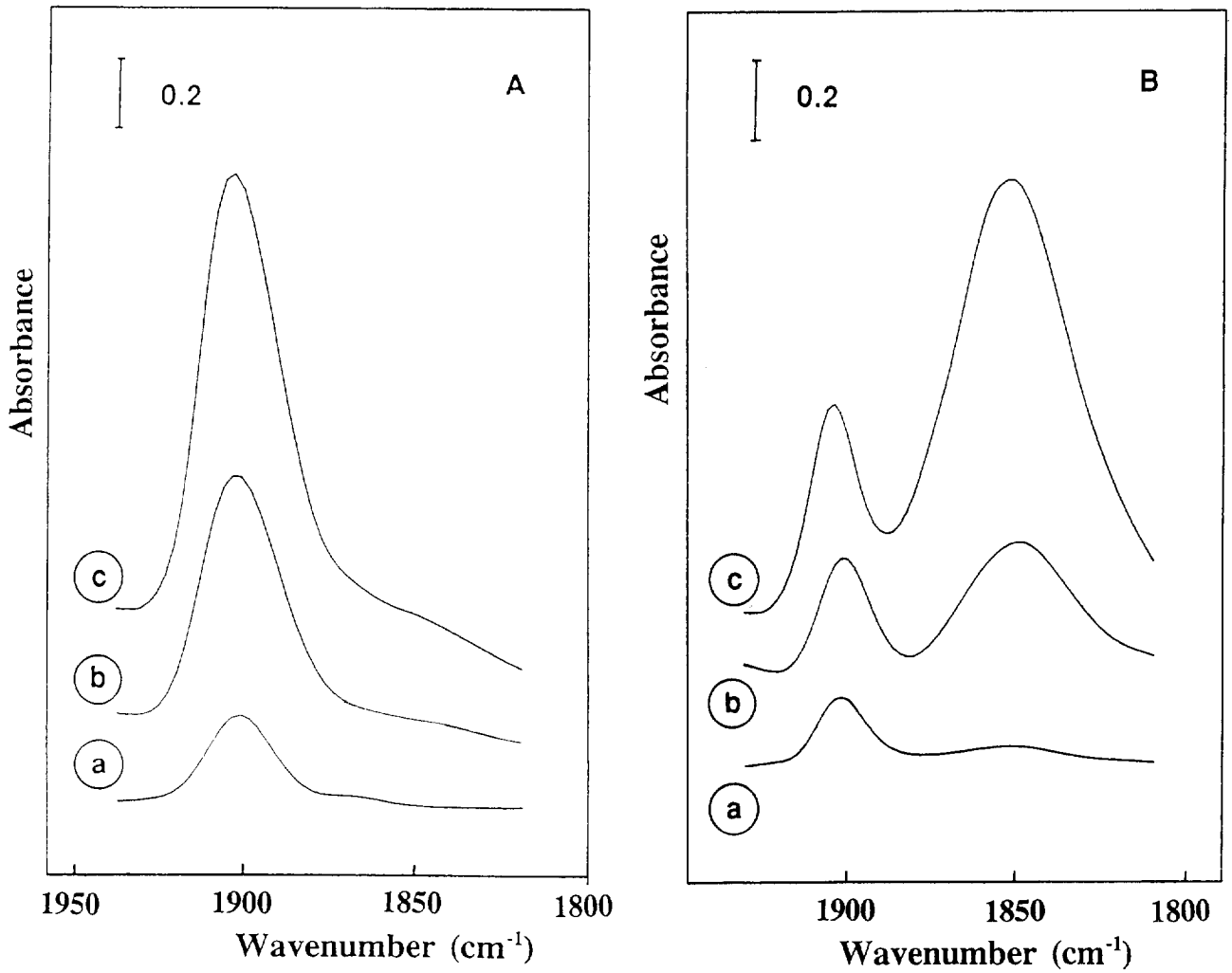

Figure 3 i.r. spectra of chemisorbed NO on unsulfided (A) and sulfided (B) *x*Ni USY zeolites: (a), 1.4 Ni; (b), 5.0 Ni; and (c), 9.0 Ni. The net spectra were obtained by subtracting the background spectra of the zeolite from the overall spectra after NO adsorption.

the stretching vibration of NO chemisorbed on sulfided Ni^{2+} ions,[11] whereas the former is due, as noted above, to NO adsorbed on unsulfided Ni^{2+} ions. This finding indicates clearly that a fraction of nickel remains as a nonsulfided Ni species. It is observed in *Figure 3B* that upon increasing the Ni content the band at 1850 cm^{-1} shifts slightly toward higher wavenumbers. For the 1,900-cm^{-1} band of the 1.4 Ni and 9.0 Ni samples the exact band positions varied between precursor and sulfided samples and were (values in parentheses for the sulfided samples): 1,902 (1,903) cm^{-1} for 1.4 Ni and 1,901 (1,904) cm^{-1} for 9.0 Ni. From these values it seems that sulfidation leads to a slight shift (large for the 9.0 Ni sample) to higher wavenumbers of the NO frequency. The exception is the 5.0 Ni sample for which this band position at 1,902 cm^{-1} was the same for both precursor and sulfided samples. Additionally, the increase of the absorbance at ca. 1,900 cm^{-1} with increasing Ni content in sulfided samples suggests that the fraction of nonsulfidable nickel increases with increasing Ni content. This finding can be taken as conclusive that a fraction of the Ni^{2+} ions present in the precursor samples cannot be sulfided under the conditions used in this study.

Photoelectron spectroscopy

The Ni $2p_{3/2}$ core level spectra of precursor and sulfided *x*Ni samples were recorded to get an idea on the nature of exposed nickel species. *Figure 4, A* and *B*, display the series of precursor and sulfided *x*Ni USY spectra, respectively, whereas *Tables 2* and *3* compile the binding energies of the Ni $2p_{3/2}$ peak along with the Ni/Si atomic ratios. The spectra show primary satellite peaks around 862.5 eV due to shake-up electrons. Wherever the line shape of the Ni $2p_{3/2}$ peak was unsymmetrical and broad we have used an empirical method to roughly resolve the curve using an expression for Gaussian/Lorentzian distribution. Upon curve fitting, the 1.4 Ni zeolite shows a Ni $2p_{3/2}$ peak at 857.6 eV, which shifts to 853.4 eV upon sulfidation. The two oxidic zeolites with a higher Ni content (x = 5.0 and 9.0) display two contributions at 855.4–855.6 and 856.8–857.1 eV. The former BE is associated with free NiO and the latter is associated with Ni^{2+} cations inter-

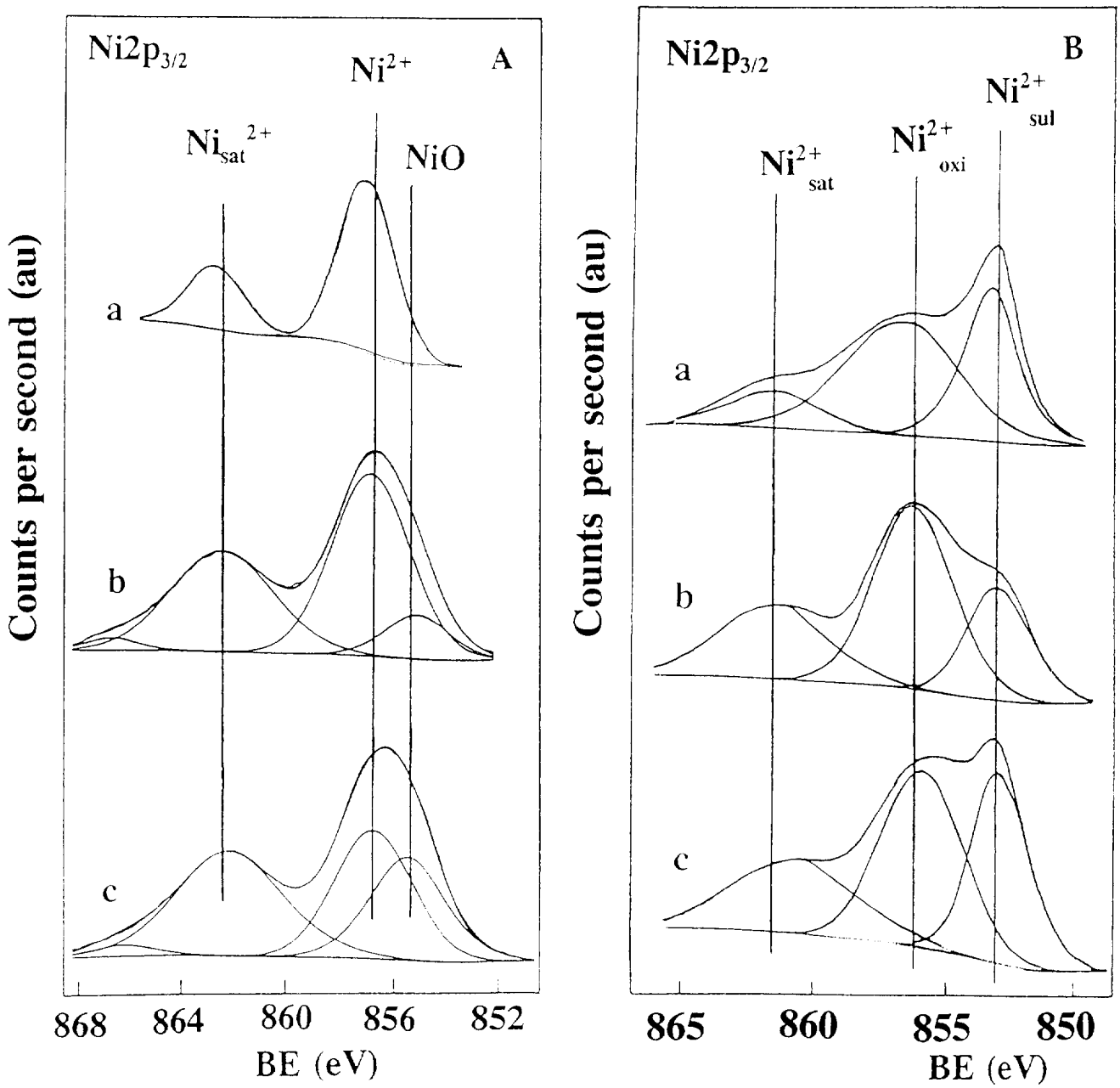

Figure 4 $Ni2p_{3/2}$ core level spectra of (A) unsulfided and (B) sulfided *x*Ni USY zeolites: (a) 1.4 Ni: (b) 5.0 Ni; and (c) 9.0 Ni.

acting with zeolite lattice oxygens,[21] and even with the EFAL produced in the zeolite with USY zeolite channels during steaming. Upon sulfiding (*Figure 4B*), two peaks at 853.0 and 855.3–855.7 eV can be discerned. The former peak corresponds to nickel sulfide (Ni_3S_2)[6], and the latter belongs, by analogy with the one found on calcined samples, to the nonsulfided Ni^{2+} species.

The S 2*p* spectral region has been also recorded for all catalysts. A single peak at ca. 161.8 eV, characteristic of S^{2-} ions,[22] was found on all sulfided catalysts. The absence of a second component at binding energies as high as 168 eV, where sulfate species are usually observed, indicates that the experimental procedure followed during sulfidation and sample transfer within the spectrometer chamber is quite efficient in avoiding air contact.

The Ni/Si XPS atomic ratios of unsulfided samples compiled in *Table 2* indicate that this ratio is extremely low for the 1.4 Ni zeolite, but it increases dramatically for 5.0 Ni and 9.0 Ni zeolites. The fast increase of the Ni/Si ratios compared to the increase in Ni loading is probably due to the covering of Si atoms from the zeolite lattice by large NiO crystals at the outer zeolite surface. The appearance of NiO diffraction lines in the X-ray diffraction pattern of the 9.0 Ni zeolite indicates NiO crystal sizes larger than ca. 5 nm. However, the crystal size of NiO in the 5.0 Ni zeolite must be small, as no diffraction lines of NiO were observed. These results

Table 2 Binding energy (eV) of core electrons and surface (XPS) atomic ratios for unsulfided xNi USY zeolites

Catalyst	Si2p	$Ni2p_{3/2}$	Ni/Si[a]
1.4 Ni	102.8	857.6	0.003
5.0 Ni	102.8	857.1 (83)[b] 855.4 (17)[b] 856.8 (56)[b]	0.259
9.0 Ni	102.8	855.6 (44)[b]	0.612

[a] Shake-up satellite Ni^{2+} was also considered in these calculations.
[b] Values in parentheses corresponded to peak percentages.

emphasize again that the Ni^{2+} ions have been ion-exchanged completely within the zeolite crystal at low Ni content (1.4 Ni zeolite) whereas oligomeric NiO structures have been developed in 5.0 Ni and 9.0 Ni catalysts. The Ni-enrichment on the zeolite surface in calcined NiHY-stabilized zeolite, prepared by ion-exchange and comparable loading to our 5.0 Ni catalyst, was also observed in the literature.[10]

The comparison of Ni/Si XPS ratios of unsulfided (*Table 2*) and sulfided (*Table 3*) samples indicates an increase in the Ni exposure for the three *x*Ni-sulfided zeolites (a factor of 11.7 for 1.4 Ni, 3.7 for 5.0 Ni, and 5.3 for 9.0 Ni samples).

Xenon adsorption and ^{129}Xe n.m.r.

Figure 5A shows the adsorption isotherms for xenon on the (oxidic) precursor samples, including pure USY. Within the pressure range studied the isotherms are almost linear, and the small deviation for the sample with the lowest Ni content does not seem significant in view of the results obtained for the other two Ni-loaded samples. One would expect a continuous decrease of the slopes of the isotherms (indicative for the Xe adsorption capacity) for samples with increasing amounts of Ni. Our observations for the oxidic samples show this behavior only rather weakly.

The adsorption isotherms for the sulfided samples are given in *Figure 5B*. The isotherms of the Ni-loaded samples all have smaller slopes than that of the parent USY sample. The smallest slope is found for 9.0 Ni (smallest adsorption capacity), whereas the slopes of 1.4 Ni and 5.0 Ni are virtually the same.

Figure 6, A and *B*, depict the ^{129}Xe chemical shift variations with Xe loading for the calcined (oxidic) samples and for the sulfided analogons, respectively. In both series clear differences exist between samples with different Ni contents and with the pure USY. For 1.4 Ni and 5.0 Ni a nonlinear chemical shift versus Xe-loading behavior is observed, whereas USY showed a linear behavior (*Figure 6A*). The corresponding single ^{129}Xe n.m.r. signals recorded for 1.4 Ni and 5.0 Ni are very broad compared with USY. The line broadening is due to the effect of paramagnetic Ni^{2+} cations and is in agreement with results observed by Gedeon et al.[23,24] for NiNaY. In the case of 9.0 Ni the ^{129}Xe n.m.r. signals were broadened beyond detection. The ^{129}Xe n.m.r. spectra of the sulfided samples consist of more than one signal: A second line is found downfield from the main signal, and one or two shoulders are found near the main signal. *Figure 6B* shows the behavior of the main signals only.

Table 3 Binding energies (eV) of core electrons and surface (XPS) atomic ratios for sulfided xNi USY zeolites

Catalyst	Si2*p*	$Ni2p_{2/3}$	S2p	Ni/Si[a]
1.4 Ni	102.9	855.8 (80)[b] 853.4 (20)[b]	161.9	0.035
5.0 Ni	102.7	855.7 (57)[b] 853.0 (43)[b]	161.9	0.966
9.0 Ni	102.6	855.3 (55)[b] 853.0 (45)[b]	161.7	3.252

[a] The shake-up satellite for both peaks of Ni^{2+} (sulfided and unsulfided) were also considered in these calculations.
[b] The values in parentheses correspond to peak percentages.

DISCUSSION

As expected from the low ion-exchange capacity of the USY zeolite the extent of Ni exchange in this zeolite was rather small but sufficient to exchange essentially all the Ni in the 1.4 Ni zeolite. However, incorporation of larger amounts of Ni by ion-exchange and impregnation procedures (samples 5.0 and 9.0) leads to a poorly dispersed nickel oxide phase. As the nickel content increases in the 5.0 and 9.0 Ni zeolites, it can be assumed that the proportion of exchanged nickel does not change substantially but that the fraction of nickel deposited on the inner or outer surface of the zeolite crystals increases. As confirmed by all the characterization data the two different preparation methods and the severe calcination conditions led to a different Ni distribution in the macro- and mesopores of the zeolite and result in the formation of some NiO on the outer surface. Water and N_2 adsorption indicate a small change of the volumes for the three *x*Ni (x = 1.4, 5.0, and 9.0) zeolites, and the volumes indicate that the porous structure of the zeolite is not blocked by the nickel oxide precursor. This finding suggests that for the *x*Ni zeolites with highest Ni content (5.0 Ni and 9.0 Ni) an important fraction of nickel is located at the outer surface of the zeolite crystals. Ezzamarty et al.[10] found a similar behavior for an NiHY catalyst with comparable Ni loading to our 5.0 Ni sample, although it was prepared only by ion-exchange.

As revealed by the i.r. spectra of chemisorbed NO, the distribution of Ni species inside the zeolite crystals differs markedly for the oxidic and sulfided *x*Ni samples with low and high nickel content. The comparison of i.r. spectra of NO chemisorbed on oxidic (*Figure 3A*) and sulfided (*Figure 3B*) *x*Ni zeolites clearly shows that a fraction of Ni^{2+} ions located at sites I, I′, and II″ is accessible to the NO probe and that they cannot be completely sulfided under the conditions used in this study. Notice that the selective titration of unsulfided (band at ca. 1,900 cm^{-1}) and sulfided (band at ca. 1,850 cm^{-1}) Ni species in a single chemisorption experiment (cf. *Figure 3B*) provides a fast and accurate method to distinguish not only the surface of unsulfided and sulfided Ni^{2+} species, but also their relative proportions. As the absorbance of NO is proportional to the number of Ni^{2+} ions accessible to NO, it is clear that the pro-

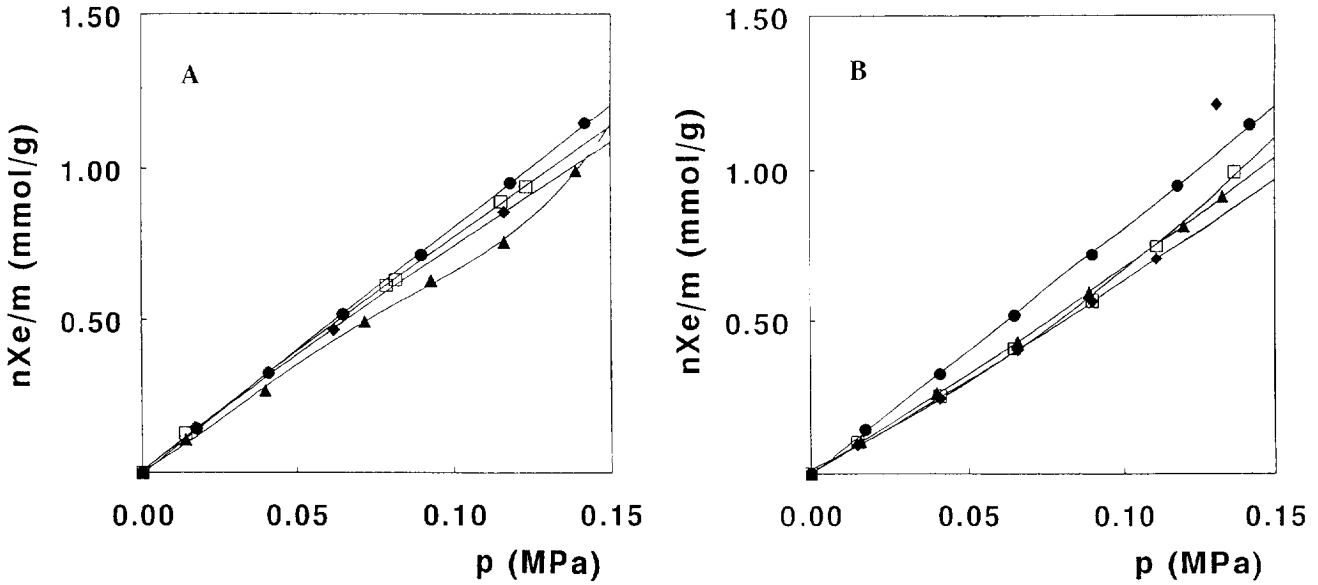

Figure 5 Adsorption isotherms of Xe on *x*Ni USY zeolites: (A) unsulfided samples; (B) sulfided samples: (●), USY; (▲), 1.4 Ni; (■), 5.0 Ni; and (♦), 9.0 Ni.

portion of exposed Ni^{2+} increased dramatically for the 5.0 Ni and 9.0 Ni zeolites. A similar tendency can be obtained from the comparison of the XPS data. Although the XPS technique is not so much surface sensitive compared to NO chemisorption and its analysis depth within the zeolite crystal is confined to 1–2 nm, the data in the last column of *Tables 2* and *3* point also to a large increase of nickel species distributed over the inner and outer zeolite surface. The combined NO chemisorption and XPS results show that during sulfidation of the 5.0 Ni and 9.0 Ni zeolite samples most of the Ni incorporated becomes sulfided but that a significant Ni fraction still remains unsulfided. It is likely that only those Ni species present in the meso-/macropores, the supercages, and perhaps the sodalite cages are relatively easy sulfidable, whereas the Ni species that (during calcination) moved to the less accessible hexagonal prisms or reacted with EFAL to form $NiAl_2O_4$ are more difficult to sulfide.

The much higher absorbances of chemisorbed NO and the Ni/Si XPS ratios in sulfided zeolites than in the oxidic counterparts point to an increase of the nickel dispersion during sulfidation. As for the 1.4 Ni zeolite most of the nickel has been ion-exchanged with the protons of the zeolite, and the large increase of the Ni/Si XPS ratio upon sulfidation suggests that a fraction of the Ni^{2+} ions moves from hidden locations, mainly in the hexagonal prisms, to more accessible po-

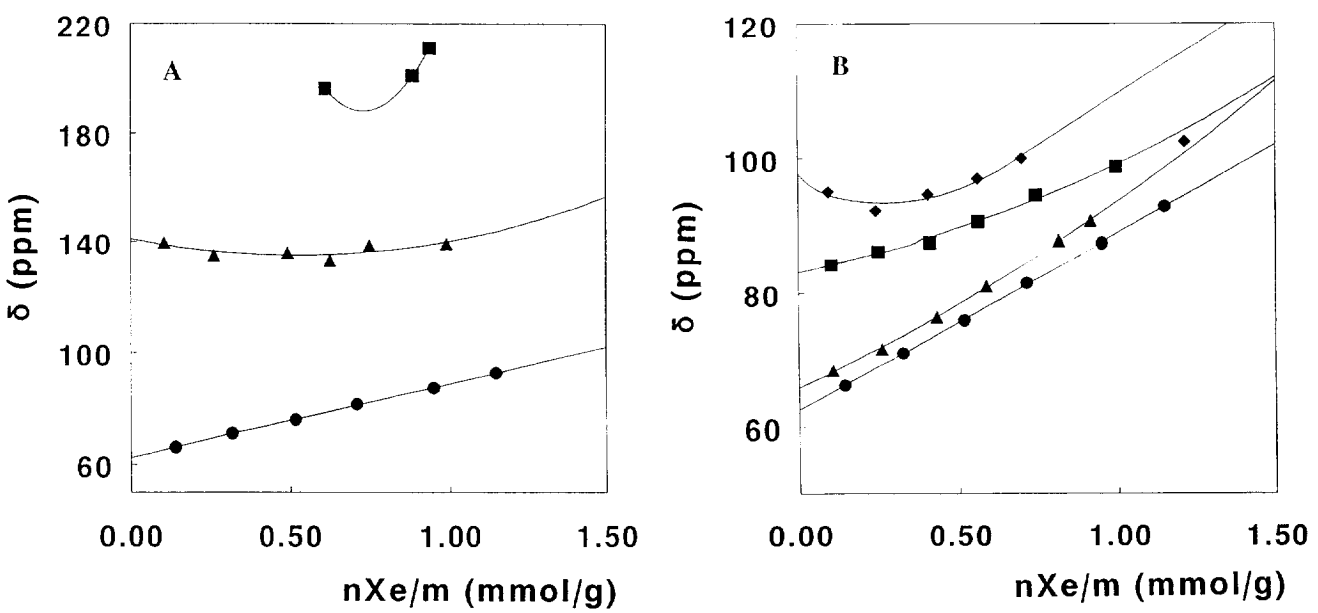

Figure 6 Chemical shift for Xenon adsorption on NiUSY zeolites: (A) unsulfided samples; and (B) sulfided samples. The symbols are the same as in *Figure 5*.

sitions. Although the Ni dispersion in 1.4 Ni zeolite seems to be complete, there is underestimation of the Ni/Si XPS ratio as a consequence of the limited escape depth of Ni $2p_{3/2}$ photoelectrons from hidden positions of the zeolite. It is also inferred that for the 5.0 Ni and 9.0 Ni zeolites sulfidation induces redistribution of "NiO clusters" deposited in the supercages and at the outer zeolite surface. Comparison of the Ni/Si ratios in *Tables 2* and *3* indicates that sulfidation decreases the homogeneity of the catalysts and that there is no proportionality between the increase of metal loading and Ni exposure either in the oxidic or in the sulfided samples. The substantial increase of the Ni/Si XPS ratio for 5.0 Ni and 9.0 Ni sulfided samples with respect to the nonsulfided counterparts can be taken as indirect evidence of Ni enrichment at the outer zeolite surface. This is mainly due to the fact that Si $2p$ photoelectrons are underestimated as their mean free paths are on the order of the size of the Ni sulfide crystal deposited on the outer surface of the zeolite crystals. The above findings are completely in agreement with our earlier observation.[5] At that time, it was concluded from XPS experiments on ion-exchanged NiNaY zeolites that a certain Ni enrichment in the outer zeolite layers occurs after sulfidation. The formation of small NiO clusters composed of Ni atoms with 3.5-oxygen neighbors and 3-Ni second nearest neighbors was proved by EXAFS analysis of NiY zeolites treated with an aqueous NaOH solution and calcined in air at 643 K,[25] indicating that the Ni2+ ions coordinated with the framework oxygen atoms of the HY zeolite migrate inside the supercages, which provide upon calcination NiO-like structures. From the above, it is apparent that these Ni clusters are different from crystalline NiO with 6 nearest oxygen and 12 second nearest Ni neighbors. An in-depth examination of the XPS data in *Table 3* reveals a shift of 0.4 eV toward higher BE values in the Ni $2p_{3/2}$ peak for sulfided 1.4 Ni compared to its parent 5.0 Ni and 9.0 Ni samples. This shift suggests that Ni^{2+} ions in the sulfided 1.4 Ni interact strongly with the zeolite matrix, forming partially sulfided structures with no clustering of Ni sulfide due to the low Ni content. As judging from the percentages of the component of Ni $2p_{3/2}$ peak at 853.0 eV (Ni sulfide) in the sulfided zeolites, there is a substantial increase from the sample 1.4 Ni to the sample 5.0 Ni, and much less marked from 5.0 Ni to sample 9.0 Ni samples. Even with the limitations of XPS and *FT* i.r. measurements, this result roughly agrees with the ratio of NO absorbances for sulfided (band at ca. 1,850 cm^{-1}) and nonsulfided (band at ca. 1,905 cm^{-1}) Ni^{2+} ions in *Figure 3B*. For the sulfided zeolites, the presence of an important fraction of Ni^{2+} ions in an environment of oxide ions indicates a strong interaction of these Ni^{2+} ions with the zeolite lattice.

The Xe-adsorption isotherms (*Figure 5, A* and *B*) show a small, but significant, difference between Ni-loaded USY and the parent USY only for the sulfided samples (see previous section). The overall features of the isotherms in *Figure 5, A* and *B*, are reminiscent of those obtained earlier for NaY exchanged with $NiCl_2$,[4] except that for the sulfide samples the isotherms do not diverge with Ni loading. The apparent insensitivity of the adsorption isotherms of oxidic samples toward the ion-exchange of Ni^{2+} for Na^+ cations can be explained by the fact that the void volume within the supercages—the volume accessible to Xe—will hardly be influenced by the cation exchange. This is because the ions are located mainly in the smaller cavities (notably at site II in the sodalite cages) where Xe does not penetrate. On the other hand, ^{129}Xe n.m.r. chemical shifts are influenced also by Xe cation interactions taking place with Ni^{2+} close to (but not actually inside) the supercages. The available void volume decreases due to sulfidation. This is caused by sulfide formation from that part of the Ni ions initially present in the supercages and those Ni ions reallocated to the supercages during the sulfidation process, resulting in the slight but significant decrease in adsorption capacities, seen for all sulfided samples with respect to the oxidic counterparts.

The results of the ^{129}Xe measurements, summarized in *Figure 6, A* and *B*, indicate that, as for the ion-exchanged NaY systems,[4] at least a part of the Ni^{2+} ions is located in or near the supercages where it can be "sensed" by Xe. Relatively large differences are found between the samples with different Ni loading and, for the nonsulfided systems with the USY support. For the oxidic 1.4 Ni and 5.0 Ni samples a nonlinear ^{129}Xe n.m.r. chemical shift versus Xe-loading behavior is found. In the case of the oxidic sample with the highest Ni content (9.0 Ni) the ^{129}Xe n.m.r. signal was broadened beyond detection. For the sulfided systems a nonlinear chemical shift plot is obtained for the sample containing 9% Ni; all other samples yield approximately linear plots (see *Figure 6B*).

Nonlinear chemical shift plots for ^{129}Xe n.m.r. of the type, illustrated in *Figure 6, A* and *B*, are often explained by invoking strong adsorption of Xe at certain sites, together with large electric field effects and/or paramagnetic effects caused by the sites.[23,24,26] In the present case, Ni^{2+} or $Ni(OH)^+$ cations located in or near the supercages would qualify for this purpose. In the oxidic samples the cations together with the negatively charged lattice sites form systems with rather large charge separations. The combined electric effects and the strong adsorption of Xe lead to deshielding in ^{129}Xe n.m.r., according to Fraissard and Ito.[26] In sulfided samples the charge separations and hence the resulting deshielding in ^{129}Xe n.m.r. will be reduced considerably compared to the oxidic counterparts.

Discussions of the type cited above all refer to systems with well-defined pore sizes and adsorption sites. In the present case we are dealing with USY support material. Depending on the method of preparation, USY may have a rather irregular structure with a spread in pore sizes. Therefore, an alternative explanation of the nonlinear ^{129}Xe chemical shift plots based on pore-size distributions should be considered as well.

For amorphous silica, alumina, and silica-alumina nonlinear ^{129}Xe n.m.r. chemical shift plots have been published by Cheung.[27] In systems possessing a distribution in (micro)pore-sizes and having only weak adsorption sites, Xe at low pressures will be adsorbed preferentially in the smaller pores, where its ^{129}Xe n.m.r.

signal will be relatively deshielded. At higher Xe loadings, the larger pores will be occupied also. Assuming rapid exchange of Xe between the various adsorption sites at 300 K,[28] this behavior should lead to decreasing chemical shifts with increasing Xe concentration at low Xe loads and to the reverse trend at higher Xe loading. This behavior was actually observed by Cheung,[27] albeit at a reduced temperature (144 K) to enhance the effect of different adsorption propensities at different sites. An additional feature of this description is that it may explain the presence of additional lines in the ^{129}Xe n.m.r. spectra.[27]

In view of the structural irregularities of the USY support, the above-cited description mechanism may not be discounted *a priori*. Yet, the analogies between the present results and those obtained earlier for NaY-supported systems lead us to prefer an explanation of our measurements in terms of strong, electrically active adsorption sites, provided by Ni^{2+} and $NiOH^{+}$ (oxidic systems) cations.[4,26] The deviations from linearity as well as the values of the ^{129}Xe n.m.r. chemical shifts are comparable for the two cases. The decrease of the curvature in the plots after sulfidation would be hard to explain in the cage-size homogeneity picture, inasmuch as one would have to assume diminishing pore-size distributions. This seems at odds with the larger sizes of the NiS particles. In contrast, within the Fraissard concept of strong adsorption sites, diminishing electric field gradients after sulfidation would have to be invoked, which seems rather plausible.[4]

With regard to the small effect of Ni-exchange on the adsorption capacities it seems worthwhile to recapitulate that after drying the majority of the Ni^{2+} ions introduced into the USY system will be located in hexagonal prisms and in sodalite cages. Both cavities are not directly involved in the Xe-adsorption process. On the other hand, Ni^{2+} or NiOH cations at or near the surfaces of the supercages will influence the n.m.r. properties of the ^{129}Xe nuclei adsorbed in the supercages.

The results of the Xe-adsorption measurements indicate that no significant amounts of Ni-containing species are present inside the supercages of the oxidic samples. This is in accordance with the structural picture of dried, NiUSY prepared by ion-exchange, as outlined above. After sulfidation, a small number of Ni-species are located within the supercages, as can be judged from the slightly decreased adsorption capacities with respect to the USY reference. This decrease seems, however, independent of the extent of exchange. This might indicate that the maximum number of Ni species originally present in the supercages (not evident from the Xe-adsorption isotherms (see above), or which are reallocated to the supercages by the sulfidation, is already reached with the lowest Ni concentration in this study.

The ^{129}Xe n.m.r. results for the oxidic samples indicate that Ni-species (Ni^{2+} or $NiOH^{+}$) must be located very close to the supercages, because its influence is easily detected by n.m.r. Such locations are, e.g., site I (hexagonal prism) and, especially, site II′ (sodalite cages). These sites, along with site I′, have been previously identified as Ni locations after the exchange of NaY with Ni^{2+}.[29–32] The number of occupied "n.m.r.-active" sites increases with growing Ni-concentration. In ^{129}Xe n.m.r. this can be followed in a qualitative fashion only from the changing chemical shifts. In the sulfided samples the electric interaction between Ni and the ^{129}Xe nuclei are smaller, presumably induced by a similar mechanism as postulated earlier.[4] An alternative explanation of the curved chemical shift plots in terms of a distribution in pore size[28] was, although not dismissed *a priori*, considered less likely.

CONCLUSION

The combined use of i.r. spectroscopy of NO, photoelectron spectroscopy, water and nitrogen sorption capabilities, and ^{129}Xe n.m.r. (with xenon adsorption) measurements provides some clues on the location of nickel in *x*Ni USY catalysts. The comparison of data for the oxidic and sulfided zeolites indicate that important changes in the location and distribution of nickel take place during sulfidation.

ACKNOWLEDGMENTS

This study is partially supported by the EC-Research Programme JOULE (Contracts 0049 and CT93-0409) and the Netherlands' Foundation for Chemical Research (SON), with financial aid from the Netherlands' Technology Foundation (STW). The USY zeolite was kindly supplied by Dr. R. Magnuson, CONTEKA, B.V., Surte (Sweden).

REFERENCES

1 Ward, J.W. in *Preparation of Catalysts III*, Studies in Surface Science and Catalysis, Vol. 16 (Eds. G. Poncelet, P. Grange and P.A. Jacobs) Elsevier, Amsterdam, 1983, p. 587
2 Weitkamp, J. and Ernst, S. in *Guidelines for mastering the properties of molecular sieves, relationship between the physicochemical properties of zeolitic systems and their low dimensionality. NATO ASI Series, Ser. B* 1990, **221**, 343
3 Cid, R., Villaseñor, J., Orellana, F., Fierro, J.L.G. and López Agudo, A. *Appl. Catal.* 1985, **18**, 357
4 Korànyi, T.I., van de Ven, L.J.M., Welters, W.J.J., de Haan, J.W., de Beer, V.H.J. and van Santen, R.A. *Catal. Lett.* 1993, **17**, 105
5 Cid, R., Fierro, J.L.G. and López Agudo, A. *Zeolites* 1990, **10**, 95
6 Kovacheva, P., Davidova, N. and Novakova, N. *Zeolites* 1991, **11**, 54
7 Cornet, D., Ezzamarty, A. and Hemidy, J.F. in *Proceedings of the 6th International Zeolite Conference* Guildfort, UK (Eds. D. Olson and A. Bisio) Butterworth-Heinemann, Stoneham, MA 1984, p. 377
8 Welters, W.J.J., de Beer, V.H.J. and van Santen, R.A. *Appl. Catal. A: General* 1994, **119**, 253
9 Leglise, J., Janin, A., Lavalley, J.C. and Cornet, D. *J. Catal.* 1988, **114**, 388
10 Ezzamarty, A., Catherine, E., Cornet, D., Hemidy, J.F., Janim, A., Lavalley, J.C., Leglise, J. and Meriaudeau, P. in *Zeolites: Facts, Figures, Future*, Studies in Surface Science and Catalysis, Vol. 49B (Eds. P.A. Jacobs and R.A. Van Santen) Elsevier, Amsterdam, 1989, p. 1025
11 Pawelec, B., Fierro, J.L.G., Cambra, J.F., Güemez, B., Duque, F. and Arias, P.L. *Bull. Soc. Chim. Belg.* 1991, **100**, 915
12 Welters, W.J.J., Vorbeck, G., Zandbergen, H.W., de Haan,

J.W., de Beer, V.H.J. and van Santen, R.A. *J. Catal.* 1994, **150,** 155
13 Welters, W.J.J., van der Waerden, O.H., de Beer, V.H.J. and van Santen, R.A. *Ind. Eng. Chem. Res.* 1995, **34,** 1166
14 Suzuki, M., Tsutsumi, K. and Takahashi, H. *Zeolites* 1982, **2,** 87
15 Laniecki, M. and Zmierczak, W. *Zeolites* 1982, **11,** 18
16 Simonot-Grange, M.-H., Elm'Chaouri, A., Weber, G., Dufresne, P., Raatz, F. and Joly, J.-F. *Zeolites* 1992, **12,** 155
17 Li, C.Y. and Rees, L.V.C. *Zeolites* 1986, **6,** 217
18 Wiśniewski, K.E. and Wojsz, R. *Zeolites* 1992, **12,** 37
19 Caceres, C., Fierro, J.L.G., Lopez Agudo, A., Severino, F. and Laine, J. *J. Catal.* 1986, **97,** 219
20 Fierro, J.L.G., Cuevas, R., Ramírez, J. and López Agudo, A. *Bull. Soc. Chim. Belg.* 1991, **100,** 945
21 Narayanan, S., 1984. *Zeolites* 1984, **4,** 231
22 In *Practical Surface Analysis. Auger and X-ray Photoelectron Spectroscopy,* (Briggs, D. and Seah, M.P., Eds.) Wiley, New York/Salle and Sauerländer, 1990, p. 607
23 Gedeon, A., Bonardet, J.L. and J. Fraissard, J. *J. Chim. Phys.* 1988, **85**(9), 871
24 Gedeon, A., Bonardet, J.L., Ito, T. and Fraissard, J. *J. Phys. Chem.* 1989, **93,** 2563
25 Sano, M., Maruo, T., Yamatera, H., Suzuki, M. and Saito, Y. *J. Am. Chem. Soc.* 1987, **109,** 52
26 Fraissard, J. and Ito, T. *Zeolites* 1988, **8,** 350
27 Cheung, T.T.P. *J. Phys. Chem.* 1989, **93,** 7549
28 Ratcliffe, C.I. and Ripmeester, J.A. *J. Am. Chem. Soc.* 1995, **117,** 1445
29 Jacobs, W.P.J.H., PhD Thesis, Eindhoven University of Technology, 1993
30 Dooryhee, E., Greaves, G.N., Steel, A.T., Townsend, R.P., Carr, S.W., Thomas, J.M. and Catlow, C.R.A. *Faraday Discuss. Chem. Soc.* 1990, **89,** 119
31 Egerton, T.A., Hagan, A., Stone, F.S. and Vickerman, J.C. *J. Chem. Soc. Faraday Trans. I* 1972, **68,** 723
32 Han, J.D. and Woo, S.I. *J. Chem. Soc. Faraday Trans. I* 1992, **88,** 145